

Hyperparallel optical quantum computation assisted by atomic ensembles embedded in double-sided optical cavities

Tao Li (李涛)¹ and Gui-Lu Long (龙桂鲁)^{1,2,3,*}¹*State Key Laboratory of Low-Dimensional Quantum Physics and Department of Physics, Tsinghua University, Beijing 100084, China*²*Tsinghua National Laboratory of Information Science and Technology, Beijing 100084, China*³*Collaborative Innovation Center of Quantum Matter, Beijing 100084, China*

(Received 8 April 2016; published 31 August 2016)

We propose an effective, scalable, hyperparallel photonic quantum computation scheme in which photonic qubits are hyperencoded both in the spatial degrees of freedom (DOF) and the polarization DOF of each photon. The deterministic hyper-controlled-NOT (hyper-CNOT) gate on a two-photon system is attainable with our interesting interface between the polarized photon and the collective spin wave (magnon) of an atomic ensemble embedded in a double-sided optical cavity, and it doubles the operations in the conventional quantum CNOT gate. Moreover, we present a compact hyper-CNOT^N gate on $N + 1$ hyperencoded photons with only two auxiliary cavity-magnon systems, not more, and it can be faithfully constituted with current experimental techniques. Our proposal enables various applications with the hyperencoded photons in quantum computing and quantum networks.

DOI: [10.1103/PhysRevA.94.022343](https://doi.org/10.1103/PhysRevA.94.022343)

I. INTRODUCTION

Quantum computation, along with quantum information processing, has attracted much attention in recent decades, partly because of its promising superfast factoring character and its potential for the efficient simulation of quantum dynamic process [1]. Some critical two-qubit gates, such as controlled-phase-flip (CPF) gate, controlled swap gate, and controlled-NOT (CNOT) gate, together with simple one-qubit rotations, can realize universal quantum computation [2]. In other words, quantum computation can be referred to as a succession of nontrivial two-qubit quantum gates and some single-qubit quantum gates. To obtain the actual physical implementation of quantum computation, one needs precise control operations on well-defined two-level quantum systems. Quantum computing with special physical systems has been extensively researched theoretically and experimentally, such as nuclear magnetic resonance [3–5], superconducting qubits [6,7], quantum dots [8–10], photons in the polarization degree of freedom (DOF) [11–15] and in both the polarization and the spatial-mode DOFs (hyperparallel photonic quantum computing) [16–18], microwave-photon resonators [19–21], and diamond nitrogen-vacancy centers [22,23].

The optical system is especially fascinating for quantum computation, since the optical qubits are ideal carriers for transmitting quantum information and can be scaled up to deal with truly large-scale quantum computation. Among all the quantum computation schemes operating with photonic qubits, they can be roughly divided into two large categories [12]. One makes use of linear optical elements and high-efficiency single-photon detectors, and the other is performed with Kerr nonlinearities. In 1998, Cerf *et al.* [24] encoded both the spatial DOF and the polarization DOF of a single photon as qubits, and a CNOT gate with the spatial DOF of the photon as the control qubit, and its polarization as the target one was

achieved. In 2000, Knill *et al.* [13] gave out a linear quantum computation scheme based on projective measurements with photon detectors and feedback operations in a probabilistic way. To constitute the critical two-qubit optical gate in a deterministic way, one can resort to Kerr nonlinearities. However, naturally occurring nonlinearities are many orders of magnitude too small for efficient quantum computation in the single-photon level [25]. Several proposals based on Kerr nonlinearities in fibers or crystals [26], electromagnetically induced transparency (EIT) [27–29], and optical cavity-dipole system [30,31] are developed. In the EIT scheme, the two single-photon pulses propagate ultraslowly through a resonant media subjected to EIT and could be mapped into two highly excited Rydberg states [32] that interact strongly with each other via dipole-dipole potential, and then a two-qubit CPF gate between the two pulses is achieved when leaving the media [27]. As for the cavity-based scheme, the dipole embedded in the optical cavity interacts strongly with the input single photons, and the interaction between the dipole and the successive photons provides strong Kerr nonlinearities that can be used to implement a CPF gate [31] on two single photons. Recently, Ren *et al.* [16–18] proposed some pioneering schemes for the hyperparallel photonic quantum computing assisted by cavity-QED systems, and they can be used to perform more quantum operations with less resources in the quantum information protocols with multiqubit systems in several DOFs, which may depress the resources consumed and the photonic dissipation [18].

Here, with the state-of-art of ultracold atomic ensembles coupling to the radiation field inside a high-finesse resonator [33–36], we put forward an alternative setup for deterministic hyperparallel optical quantum computation. Other than a two-qubit CPF gate on the successive single-photon pulses [31], we make use of the cavity-based scheme to constitute a hyper-CNOT gate on two hyperencoded single photons. Both the spatial DOF and the polarization DOF are utilized to encode qubits as Cerf *et al.* [24] did in their linear quantum computation protocol. Instead of taking the spatial DOF as

*Corresponding author: gllong@mail.tsinghua.edu.cn

the control qubit and taking the polarization as the target, the spatial and polarization DOFs of the control photon are independently used to control the spatial and polarization DOFs of the target photon, respectively. Compared with the initial single-sided cavity-based optical quantum computation schemes [14,30,31], our proposal has the following advantages: (i) our optical quantum computation is hyperparallel, and each photon is encoded with two qubits, namely, the spatial qubit $\{|a_1\rangle, |a_2\rangle\}$ and the polarization qubit $\{|H\rangle, |V\rangle\}$, which is more powerful and more efficient [16–18]; (ii) the atomic ensemble can offer a multimode quantum storage media for the hyperencoded photons, and it will lead to a potentially fast readout procedure when the quantum memory for polarized photon qubit is needed; in addition, (iii) the spatial CNOT (S-CNOT) gate and the polarization CNOT (P-CNOT) gate can be performed independently, and the multiqubit hyper-CNOT^{*N*} gates can be in principle achieved. In other words, our hyperparallel scheme is scalable and can be useful for hyperencoded optical quantum computation.

The paper is organized as follows. In Sec. II, we focus on the input-output relation for a single photon with our atomic ensemble embedded in a double-sided microcavity which yields the desired Kerr nonlinearity. The heralded hyper-CNOT gate on two photons is constructed in Sec. III, and its performance is briefly discussed with the current experimental techniques. Besides, we also give out the multiqubit hyper-CNOT^{*N*} gate on $N + 1$ hyperencoded photons in Sec. III. Finally, we end up with some discussion on the experimental feasibility of our scheme and a summary in Sec. IV.

II. INPUT-OUTPUT RELATION FOR A SINGLE PHOTON WITH AN ATOMIC ENSEMBLE EMBEDDED IN A DOUBLE-SIDED CAVITY

The relevant level structure of the ⁸⁷Rb [37,38], i.e., $5S_{1/2}$ and $5P_{1/2}$ manifolds involved and a highly excited Rydberg state $nS_{1/2}$ denoted $|r\rangle$, is shown in Fig. 1. Assisted by the Rydberg state $|r\rangle$, one can prepare the atomic ensemble into the single-excited collective spin wave (magnon) state and perform the single-qubit operation on the magnon qubits. Initially all the atoms are pumped to the state $|g\rangle = |5S_{1/2}, F = 2, M_F = 0\rangle$. The collective spin wave state or magnon state

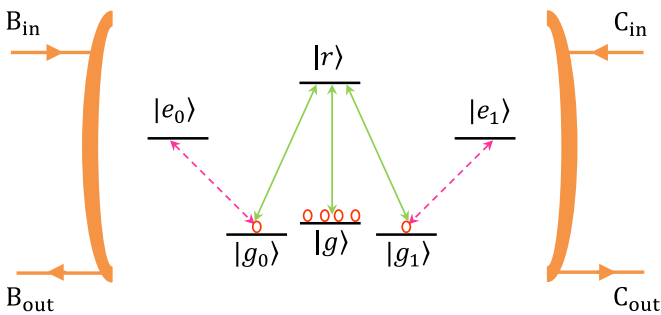


FIG. 1. Schematic diagram of the atomic ensemble cavity coupling system. The incoming photon in port *B* will be totally reflected when the coupling between the atomic ensemble and the cavity is switched on, whereas, totally transmitted into port *C* when the coupling is switched off.

with a single atom in the state $|g_0\rangle = |5S_{1/2}, F = 1, M_F = -1\rangle$ and $|g_1\rangle = |5S_{1/2}, F = 1, M_F = 1\rangle$ are exploited to encode the magnon qubit and can store the orthogonally polarized photon. The single excited collective state can be represented by $|c^s\rangle = \frac{1}{\sqrt{N}} \sum_{j=1}^N |g^1, \dots, c^j, g^{j+1}, \dots, g^N\rangle$, which means that all atoms are in state $|g\rangle$ except for the j th one in state $|c\rangle$ ($|c\rangle = |g_0\rangle, |g_1\rangle, |e_0\rangle, |e_1\rangle$, or $|r\rangle$, where $|e_0\rangle = |5P_{1/2}, F = 2, M_F = -2\rangle$, $|e_1\rangle = |5P_{1/2}, F = 2, M_F = 2\rangle$, and $|r\rangle = |nS\rangle$). The transitions $|g_0^s\rangle \leftrightarrow |e_0^s\rangle$ and $|g_1^s\rangle \leftrightarrow |e_1^s\rangle$ with frequency ω_0 are nearly resonantly coupled to the two degenerate cavity modes \hat{a}_0 and \hat{a}_1 with orthogonal polarizations *H* and *V*, respectively (shown in Fig. 1), and the corresponding coupling rates are λ_0 and λ_1 . Meanwhile, the two cavity modes \hat{a}_0 and \hat{a}_1 of the frequency ω_a are nearly resonantly driven by *H* and *V* polarized photons input into the cavity, respectively. The state of the ensemble will provide an appreciable difference in the transmission and reflection coefficients for the input photons with different polarizations. For instance, an *H* polarized photon input from either side of the cavity will pass through the cavity if the ensemble is in the state $|g_1^s\rangle$, since the ensemble is decoupled from the driven cavity mode \hat{a}_0 . However, for the ensemble in the state $|g_0^s\rangle$, it will interact with the *H* photon and lead to the mode splitting of the cavity, resulting in the perfect reflection of *H* photon in the ideal case.

Consider a single polarized photon pulse with a finite bandwidth $[\omega_a - \Delta/2, \omega_a + \Delta/2]$, $\Delta \ll \kappa$ (the cavity decay rate), and the coupling rates between an asymmetrical cavity and modes $\hat{b}_i(\omega)$ and $\hat{c}_i(\omega)$ of ports *B* and *C* taken as real constant, denoted $\sqrt{\kappa_b}/2\pi$ and $\sqrt{\kappa_c}/2\pi$, respectively, since only the optical fields with frequency close to the cavity frequency ω_a contribute mostly to the cavity mode [31]. Here we choose ω_a as the carrier frequency, and $\delta' = \omega - \omega_a$ measures the frequency detuning of ω component of the input photon. $\delta_0 = \omega_0 - \omega_a$ denotes the frequency difference between the dipole transition and the cavity mode. The Hamiltonian of the system in the frame rotating with respect to ω_a is [39]

$$\begin{aligned} \hat{H} = \sum_{i=0,1} \left\{ \left(\delta_0 - \frac{i\gamma_{e_i}}{2} \right) \hat{\sigma}_{e_i e_i} + i\lambda_i (\hat{a}_i \hat{\sigma}_{g_i e_i}^\dagger - \hat{a}_i^\dagger \hat{\sigma}_{g_i e_i}) \right. \\ + \int_{-\frac{\Delta}{2}}^{\frac{\Delta}{2}} \delta' d\delta' \hat{b}_i^\dagger(\delta') \hat{b}_i(\delta') + \int_{-\frac{\Delta}{2}}^{\frac{\Delta}{2}} \delta' d\delta' \hat{c}_i^\dagger(\delta') \hat{c}_i(\delta') \\ + i\sqrt{\frac{\kappa_b}{2\pi}} \int_{-\frac{\Delta}{2}}^{\frac{\Delta}{2}} d\delta' [\hat{b}_i^\dagger(\delta') \hat{a}_i - \hat{b}_i(\delta') \hat{a}_i^\dagger] \\ \left. + i\sqrt{\frac{\kappa_c}{2\pi}} \int_{-\frac{\Delta}{2}}^{\frac{\Delta}{2}} d\delta' [\hat{c}_i^\dagger(\delta') \hat{a}_i - \hat{c}_i(\delta') \hat{a}_i^\dagger] \right\}. \quad (1) \end{aligned}$$

Here γ_{e_i} and λ_i denote the spontaneous emission rate of the single excited collective state $|e_i^s\rangle$ and the coupling rate between the atomic ensemble and the corresponding resonant cavity modes, respectively. $\hat{\sigma}_{e_i e_i} = |e_i^s\rangle\langle e_i^s|$ and $\hat{\sigma}_{g_i e_i} = |g_i^s\rangle\langle e_i^s|$. When the atomic ensemble is pumped to the magnon state $|g_i^s\rangle$ with the help of Rydberg state [32,40] or coherent Raman process [41,42], a polarized photon either in mode \hat{b}_i or \hat{c}_i directed into the cavity will drive the interaction between the atomic ensemble and the cavity. In the single excitation subspace, the composite system composed of the

atomic ensemble and three radiation modes could evolve into a general state $|\Psi(t)\rangle$ with the Hamiltonian \hat{H} [43,44],

$$|\Psi(t)\rangle = \sum_{i=0,1} \left[\alpha_i(t) |g_i^s, 1, 0, 0\rangle + \int d\delta' \beta_i(\delta', t) |g_i^s, 0, 1, 0\rangle + \int d\delta' \varepsilon_i(\delta', t) |g_i^s, 0, 0, 1\rangle + \zeta_i(t) |e_i^s, 0, 0, 0\rangle \right], \quad (2)$$

where the four dimensions of each ket $|\Psi(t)\rangle$ are spanned by the internal states of the atomic ensemble and the photon number states of the radiation modes (\hat{a}_i , \hat{b}_i , and \hat{c}_i), respectively.

The Schrödinger equation for this system can be specified to be

$$\begin{aligned} i\dot{\beta}_i(\delta', t) &= \delta' \beta_i(\delta', t) + i\sqrt{\frac{\kappa_b}{2\pi}} \alpha_i(t), \\ i\dot{\varepsilon}_i(\delta', t) &= \delta' \varepsilon_i(\delta', t) + i\sqrt{\frac{\kappa_c}{2\pi}} \alpha_i(t), \\ i\dot{\zeta}_i(t) &= i\lambda_i \alpha_i(t) + \left(\delta_0 - i\frac{\gamma_{e_i}}{2} \right) \zeta_i(t), \\ i\dot{\alpha}_i(t) &= -i\lambda_i \zeta_i(t) - i\sqrt{\frac{\kappa_b}{2\pi}} \int_{-\frac{\Delta}{2}}^{\frac{\Delta}{2}} d\delta' \beta_i(\delta', t) \\ &\quad - i\sqrt{\frac{\kappa_c}{2\pi}} \int_{-\frac{\Delta}{2}}^{\frac{\Delta}{2}} d\delta' \varepsilon_i(\delta', t). \end{aligned} \quad (3)$$

As the equations for different polarized photons are decoupled, one can solve them individually with respect to the polarization of the photon input. To clarify the birefringent character of the system composed of the atomic ensemble and double-sided cavity, referred as cavity-magnon system below, we choose the input photon in mode \hat{b}_i and the initial state $|\Psi(0)\rangle = |g_i^s, 0, 1, 0\rangle$. Along with the standard input-output relation [39] $\hat{y}_i^{\text{out}} = \hat{y}_i^{\text{in}} + \sqrt{\kappa_y} \hat{a}_i$ ($y = b, c$ and $i = 0, 1$), the reflection and the transmission coefficients $r^a(\omega)$ and $t^a(\omega)$ with the input photon in mode \hat{b}_i , in the weak excitation approach, can be detailed, respectively, by

$$\begin{aligned} r^a(\omega) &= \frac{[i(\omega_a - \omega) + \frac{\kappa_c - \kappa_b}{2}][i(\omega_0 - \omega) + \frac{\gamma_{e_i}}{2}] + \lambda_i^2}{[i(\omega_a - \omega) + \frac{\kappa_b + \kappa_c}{2}][i(\omega_0 - \omega) + \frac{\gamma_{e_i}}{2}] + \lambda_i^2}, \\ t^a(\omega) &= \frac{-\sqrt{\kappa_b \kappa_c} [i(\omega_0 - \omega) + \frac{\gamma_{e_i}}{2}]}{[i(\omega_a - \omega) + \frac{\kappa_b + \kappa_c}{2}][i(\omega_0 - \omega) + \frac{\gamma_{e_i}}{2}] + \lambda_i^2}. \end{aligned} \quad (4)$$

As for the case that the cavity mode driven is decoupled from the atomic ensemble, the coupling rate $\lambda_i = 0$, one can get the specific reflection and transmission coefficients,

$$\begin{aligned} r_0^a(\omega) &= \frac{i(\omega_a - \omega) + \frac{\kappa_c - \kappa_b}{2}}{i(\omega_a - \omega) + \frac{\kappa_b + \kappa_c}{2}}, \\ t_0^a(\omega) &= \frac{-\sqrt{\kappa_b \kappa_c}}{i(\omega_a - \omega) + \frac{\kappa_b + \kappa_c}{2}}. \end{aligned} \quad (5)$$

To obtain the reflection and transmission coefficients with the input photon in mode \hat{c}_i , one just needs to exchange κ_b and κ_c according to the symmetric character in this cavity-magnon system.

When the coupling rates between the cavity and the modes $\hat{b}_i(\omega)$ and $\hat{c}_i(\omega)$ are of small difference $\kappa_\Delta = |\kappa_c - \kappa_b| \ll$

κ_{\min} ($\kappa_{\min} = \min\{\kappa_b, \kappa_c\}$), one can replace the reflection and transmission coefficients above for the asymmetrical cavity system with those for the symmetrical one with identical coupling rates $\kappa = \kappa_b = \kappa_c$. Meanwhile, it will introduce an additional error probability ϵ in the single-photon scattering process by $\epsilon \sim \max\{\kappa_\Delta^2/(\kappa_b + \kappa_c)^2, \kappa_\Delta^2 \gamma_{e_i}^2/\lambda_i^4\}$ in the resonant case, and this can be improved by the use of the cavity with almost identical mirrors [45,46], which will lead to the ideal photon blockade [47] and two-photon gateway [48]. With the symmetrical cavity, the corresponding reflection and transmission coefficients for the coupling and decoupling cases can be respectively simplified as

$$\begin{aligned} r(\omega) &= 1 + t(\omega), \\ t(\omega) &= \frac{-\kappa [i(\omega_0 - \omega) + \frac{\gamma_{e_i}}{2}]}{[i(\omega_a - \omega) + \kappa][i(\omega_0 - \omega) + \frac{\gamma_{e_i}}{2}] + \lambda_i^2} \end{aligned} \quad (6)$$

and

$$\begin{aligned} r_0(\omega) &= 1 + t_0(\omega), \\ t_0(\omega) &= \frac{-\kappa}{i(\omega_a - \omega) + \kappa}. \end{aligned} \quad (7)$$

From these expressions, one can draw a conclusion that if the bandwidth of the input photon pulse is narrow enough $\Delta/2 \ll \kappa$ and the spontaneous coefficient γ_{e_i} is small enough when it is compared with the cavity character $2\lambda_i^2/\kappa$, the reflection coefficient $r(\omega) \simeq 1$ and the transmission coefficient $t(\omega) \simeq 0$. However, the input photon, in the decoupling case ($\lambda_i = 0$), could also be output in a nearly deterministic mode, since $t_0(\omega) \simeq -1$ and $r_0(\omega) \simeq 0$, when the photon is nearly resonant to the cavity mode ($\omega_a - \omega \simeq 0$).

When two single-photon pulses are successively directed into the cavity, a π phase shift will appear if the polarization states of the photons are different, but a *zero* phase shift appears for two photons with the same polarization. However, in both cases, whether the photon is reflected or transmitted is determined by the state of the atomic ensemble. This exactly demonstrates the effective Kerr nonlinearity which can be used to constitute the hyper-CNOT gate in the following section.

III. HYPERPARALLEL GATES BASED ON THE EFFECTIVE KERR NONLINEARITY

With an atomic ensemble embedded in a two-sided optical cavity, the output process of the single polarized photon performs the birefringence character, which is dependent on the internal state of the atomic ensemble. Now, we proceed to present the detailed scheme of our hyper-CNOT gate on two photons a and b both hyperencoded in the polarization and the spatial-mode DOFs. That is, a hyper-CNOT gate performs both the CNOT gate on the state of the two-photon system in the polarization DOF (P-CNOT) and that in the spatial-mode DOF (S-CNOT). Suppose the states of a and b are, respectively, $|\varphi\rangle_a$ and $|\varphi\rangle_b$

$$\begin{aligned} |\varphi\rangle_a &= |\varphi\rangle_{a_s} \otimes |\varphi\rangle_{a_p}, \\ |\varphi\rangle_b &= |\varphi\rangle_{b_s} \otimes |\varphi\rangle_{b_p}. \end{aligned} \quad (8)$$

Here

$$\begin{aligned} |\varphi\rangle_{a_s} &= \alpha_1|a_1\rangle + \alpha_2|a_2\rangle, \\ |\varphi\rangle_{b_s} &= \mu_1|b_1\rangle + \mu_2|b_2\rangle, \\ |\varphi\rangle_{a_p} &= \beta_1|H\rangle + \beta_2|V\rangle, \\ |\varphi\rangle_{b_p} &= \nu_1|H\rangle + \nu_2|V\rangle, \end{aligned} \quad (9)$$

and all of the states presented above are normalized, i.e., $|\xi_1|^2 + |\xi_2|^2 = 1$ ($\xi = \alpha, \beta, \mu,$ and ν). Meanwhile, the subscripts a and b , respectively, denote photon a and photon b , and the sub-subscripts s and p are used to abbreviate the spatial DOF and the polarization DOF of the photon involved. $|H\rangle$ and $|V\rangle$ represent two orthogonal polarization modes of photons, respectively. $|a_1\rangle$ and $|a_2\rangle$ ($|b_1\rangle$ and $|b_2\rangle$) are the two spatial modes of photon a (b). Here we take the ideal input-output process of the single photons to give out the principle of our hyper-CNOT gate. That is, an input polarized photon driving the interaction between the cavity mode and the atomic ensemble will be totally reflected by the cavity, but the orthogonal polarized one will pass through the cavity with a π phase shift, since the cavity mode driven is decoupled from the atomic ensemble.

A. P-CNOT gate based on the effective Kerr nonlinearity

The framework of our proposal for the P-CNOT gate on the two-photon system ab is shown in Fig. 2. H_i ($i = 1, 2, 3,$ and 4) represents a half-wave plate that could be used to perform the Hadamard operation $|H\rangle \rightarrow \frac{1}{\sqrt{2}}(|H\rangle + |V\rangle)$ and $|V\rangle \rightarrow \frac{1}{\sqrt{2}}(|H\rangle - |V\rangle)$ on the polarization DOF of photon a , and HWP_j ($j = 1, 2,$ and 3) stands for a half-wave plate performing the bit-flip operation $\sigma_x = |H\rangle\langle V| + |V\rangle\langle H|$. The PBS is a polarizing beam splitter which transmits the polarized photon $|H\rangle$ and reflects $|V\rangle$, respectively. Since the two photons a and b are in an arbitrary product state $|\varphi\rangle_{ab} = |\varphi\rangle_a \otimes |\varphi\rangle_b$, an ideal P-CNOT gate with the polarization DOF of photon a as

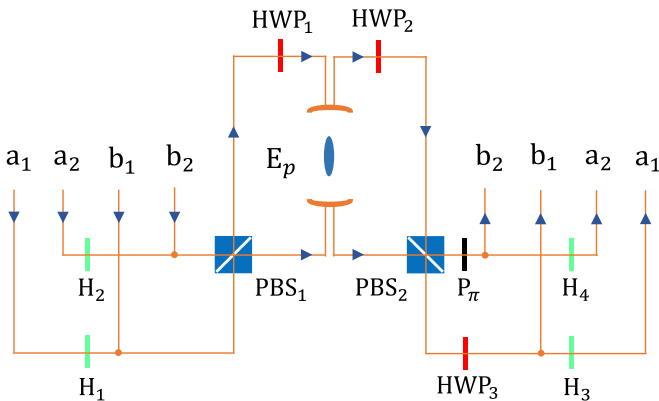


FIG. 2. Schematic diagram for the P-CNOT gate. The square brackets containing an ellipse stand for the cavity-ensemble system. HWP_i and H_j are half-wave plates whose optical axes are set differently to perform the bit-flip operation and the Hadamard operation on the polarization DOF of photons, respectively. P_π is a π phase shifter, and the PBS is a polarizing beam splitter, which transmits the $|H\rangle$ polarized photon and reflects the $|V\rangle$ polarized one, respectively.

the control qubit and that of photon b as the target qubit will transfer the state $|\varphi\rangle_{ab}$ into the state $|\varphi_p\rangle_{a\bar{b}}$. Here

$$|\varphi_p\rangle_{a\bar{b}} = |\varphi\rangle_{a_s} \otimes |\varphi\rangle_{b_s} \otimes [\beta_1|H\rangle \otimes \hat{\sigma}_{x_p} |\varphi\rangle_{b_p} + \beta_2|V\rangle \otimes |\varphi\rangle_{b_p}]. \quad (10)$$

The spatial DOF is not contaminated and the single-qubit operator performed on b is a bit-flip operation $\hat{\sigma}_{x_p} = |H\rangle\langle V| + |V\rangle\langle H|$.

To implement the transformation $|\varphi\rangle_{ab} \rightarrow |\varphi_s\rangle_{a\bar{b}}$, we first initialize the atomic ensemble E_p into a superposition state $|\varphi\rangle_m = \frac{1}{\sqrt{2}}(|g_0^s\rangle + |g_1^s\rangle)$ and then input the control photon a in the state $|\varphi\rangle_a$. After passing through the half-wave plates H_1 and H_2 , the spatial modes a_1 and a_2 of photon a are combined at the PBS_1 . With HWP_1 for the bit-flip operation performed on the a_1 mode, the state of photon a input into the cavity evolves into $|\varphi_p\rangle_1$,

$$\begin{aligned} |\varphi_p\rangle_1 &= \alpha_1(\beta'_1|a_1\rangle + \beta'_2|a_2\rangle) \otimes |V\rangle \\ &\quad + \alpha_2(\beta'_1|a_2\rangle + \beta'_2|a_1\rangle) \otimes |H\rangle. \end{aligned} \quad (11)$$

Here $\beta'_1 = \frac{1}{\sqrt{2}}(\beta_1 + \beta_2)$ and $\beta'_2 = \frac{1}{\sqrt{2}}(\beta_1 - \beta_2)$. Considering the birefringent propagation of the polarized photon input, the output state of photon a together with that of the atomic ensemble is $|\varphi_p\rangle_2$,

$$\begin{aligned} |\varphi_p\rangle_2 &= \frac{1}{\sqrt{2}} \{ \alpha_1 [\beta'_1 (|a_1\rangle|V\rangle|g_1^s\rangle - |a_2\rangle|V\rangle|g_0^s\rangle) \\ &\quad + \beta'_2 (|a_2\rangle|V\rangle|g_1^s\rangle - |a_1\rangle|V\rangle|g_0^s\rangle)] \\ &\quad + \alpha_2 [\beta'_1 (|a_2\rangle|H\rangle|g_0^s\rangle - |a_1\rangle|H\rangle|g_1^s\rangle) \\ &\quad + \beta'_2 (|a_1\rangle|H\rangle|g_0^s\rangle - |a_2\rangle|H\rangle|g_1^s\rangle)] \}. \end{aligned} \quad (12)$$

With HWP_2 for another bit-flip operation on the a_1 mode, the two spatial modes a_1 and a_2 of photon a are combined again at the PBS_2 , and then pass through HWP_3 and P_π , respectively. The state $|\varphi_p\rangle_2$ involves into

$$\begin{aligned} |\varphi_p\rangle_3 &= \frac{1}{\sqrt{2}} |\varphi\rangle_{a_s} \otimes [-(\beta'_1|H\rangle + \beta'_2|V\rangle)|g_0^s\rangle \\ &\quad + (\beta'_1|V\rangle + \beta'_2|H\rangle)|g_1^s\rangle]. \end{aligned} \quad (13)$$

$|\varphi_p\rangle_3$ is the desirable output state for a hybrid CPF gate on a photon-magnon system. The half-wave plates H_3 and H_4 , respectively, on the a_1 and a_2 modes will introduce a Hadamard operation on the polarization DOF of the photon a . If one performs a Hadamard operation H_m on the atomic ensemble, $|g_0^s\rangle \rightarrow \frac{1}{\sqrt{2}}(|g_0^s\rangle + |g_1^s\rangle)$ and $|g_1^s\rangle \rightarrow \frac{1}{\sqrt{2}}(|g_0^s\rangle - |g_1^s\rangle)$, with the coherent Raman process or Rydberg-state-assisted quantum rotation, one projects the composite system composed of the photon a and the atomic ensemble E_p into the state

$$|\varphi_p\rangle_4 = |\varphi\rangle_{a_s} \otimes [\beta_2|V\rangle|g_0^s\rangle + \beta_1|H\rangle|g_1^s\rangle], \quad (14)$$

which is a hybrid two-qubit entangled state for the system composed of photon a and the atomic ensemble E_p when $\beta_1\beta_2 \neq 0$, and it can be used to perform quantum communication and distributed quantum computation [1].

Compared with the optical path of photon a , the target photon b in the state $|\varphi\rangle_b$ passes through a relatively simple optical path where the four half-wave plates H_i ($i = 1, 2, 3,$ and 4) are removed. The Hadamard operations on the polarization

DOF of the photon are excluded; therefore, the evolution of target photon b together with control photon a and the atomic ensemble of state $|\varphi_p\rangle_4$ can be obtained with a similar way to the evolution discussed in Eqs. (12) and (13), and one has

$$|\varphi_p\rangle_5 = |\varphi\rangle_{a_s} \otimes |\varphi\rangle_{b_s} \otimes \left[-\beta_2|V\rangle|\varphi\rangle_{b_p} |g_0^s\rangle + \beta_1|H\rangle(\sigma_{x_b^p}|\varphi\rangle_{b_p})|g_1^s\rangle \right]. \quad (15)$$

After the photon b passes through the setup and propagates into the two output modes b_1 and b_2 , another Hadamard operation H_m on the atomic ensemble is performed and the state of the combined system then evolves into

$$|\varphi_p\rangle_6 = \left[(\beta_2|V\rangle \otimes |\varphi\rangle_{b_p} - \beta_1|H\rangle \otimes \sigma_{x_b^p}|\varphi\rangle_{b_p}) \otimes |g_0^s\rangle + (\beta_2|V\rangle \otimes |\varphi\rangle_{b_p} + \beta_1|H\rangle \otimes \sigma_{x_b^p}|\varphi\rangle_{b_p}) \otimes |g_1^s\rangle \right] \otimes |\varphi\rangle_{a_s} \otimes |\varphi\rangle_{b_s}. \quad (16)$$

Subsequently, the atomic ensemble state can be measured with the energy exchange-free method developed in Ref. [49] or others [50]. On detecting the atomic ensemble in state $|g_1^s\rangle$, one projects the hybrid state in Eq. (16) into the desired outcome of P-CNOT gate, shown in Eq. (10), with the polarization DOF of photon a as control qubit and that of b as target qubit. As for the $|g_0^s\rangle$ case, a single phase-flip operator $\sigma_{z_a^p} = |H\rangle\langle H| - |V\rangle\langle V|$ performed on a leads to the same result as that of $|g_1^s\rangle$. In a word, the P-CNOT gate on the two-photon system ab , in the ideal case, can be achieved deterministically in a heralded way, without any negative influence on their spatial-mode quantum states.

B. S-CNOT gate based on the effective Kerr nonlinearity

Up to now, we detailed our scheme for constructing a P-CNOT gate with the spatial DOF of the photons unpolluted. However, in order to implement the hyperparallel optical quantum computation with the qubits hyperencoded in both the spatial and the polarization DOFs of a two-photon system, an S-CNOT gate acting on the spatial DOF of the two photons involved is constituted in this subsection. Figure 3 shows the schematic diagram for the S-CNOT gate. The BS_j ($j = 1, 2$) represents the beam splitter which is used to perform the Hadamard operation $|a_1\rangle \rightarrow \frac{1}{\sqrt{2}}(|a_1\rangle + |a_2\rangle)$ and $|a_2\rangle \rightarrow \frac{1}{\sqrt{2}}(|a_1\rangle - |a_2\rangle)$ on the spatial DOF of photon a . To demonstrate the generality of our S-CNOT gate, we can choose

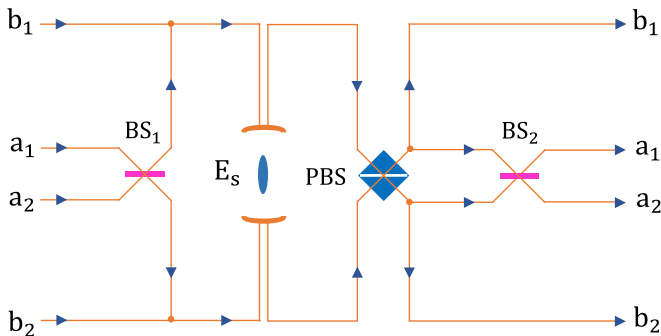


FIG. 3. Schematic diagram for the S-CNOT gate. The BS is a balanced nonpolarized beam splitter, which is used to perform the Hadamard operation on the spatial DOF of photons.

the states of photons a and b to be $|\varphi\rangle_a$ and $|\varphi\rangle_b$ in Eq. (8), respectively, as we did in constructing the P-CNOT gate.

First, one can initialize the atomic ensemble E_s in Fig. 3. to a superposition state $|\varphi\rangle_m$, and then direct the photon a into the a_1, a_2 input modes of the S-CNOT gate. The state of photon a together with the atomic ensemble E_s , i.e., $|\varphi_s\rangle_1 = |\varphi\rangle_a \otimes |\varphi\rangle_m$, evolves as

$$\begin{aligned} & \xrightarrow{BS_1} (\alpha'_1|a_1\rangle + \alpha'_2|a_2\rangle) \otimes |\varphi\rangle_{a_p} \otimes |\varphi\rangle_m \\ & \xrightarrow{\text{cavity}} \frac{1}{\sqrt{2}} \left\{ |g_0^s\rangle [\beta_1|H\rangle(\alpha'_1|a_1\rangle + \alpha'_2|a_2\rangle) - \beta_2|V\rangle(\alpha'_1|a_2\rangle + \alpha'_2|a_1\rangle)] \right. \\ & \quad \left. + |g_1^s\rangle [-\beta_1|H\rangle(\alpha'_1|a_2\rangle + \alpha'_2|a_1\rangle) + \beta_2|V\rangle(\alpha'_1|a_1\rangle + \alpha'_2|a_2\rangle)] \right\} \\ & \xrightarrow{PBS} \frac{1}{\sqrt{2}} \left\{ |g_0^s\rangle [(\beta_1|H\rangle - \beta_2|V\rangle) \otimes (\alpha'_1|a_2\rangle + \alpha'_2|a_1\rangle)] + |g_1^s\rangle [(-\beta_1|H\rangle + \beta_2|V\rangle) \otimes (\alpha_1|a_1\rangle + \alpha_2|a_2\rangle)] \right\} \\ & \xrightarrow{BS_2} \frac{1}{\sqrt{2}} \left[|g_0^s\rangle \otimes (\alpha_1|a_1\rangle - \alpha_2|a_2\rangle) - |g_1^s\rangle \otimes |\varphi\rangle_{a_s} \right] \otimes (\beta_1|H\rangle - \beta_2|V\rangle) \\ & = |\varphi_s\rangle_2, \end{aligned} \quad (17)$$

where $\alpha'_1 = \frac{1}{\sqrt{2}}(\alpha_1 + \alpha_2)$ and $\alpha'_2 = \frac{1}{\sqrt{2}}(\alpha_1 - \alpha_2)$. With a Hadamard operation H_m on the atomic ensemble E_s , $|\varphi_s\rangle_2$ evolves into the state $|\varphi_s\rangle_3$,

$$|\varphi_s\rangle_3 = (\beta_1|H\rangle - \beta_2|V\rangle)(\alpha_2|a_2\rangle|g_0^s\rangle - \alpha_1|a_1\rangle|g_1^s\rangle), \quad (18)$$

which is a hybrid entangled state, since the spatial modes of the photon a cannot be decoupled from the atomic ensemble E_s when $\alpha_1\alpha_2 \neq 0$.

After the H_m operation, one can direct the target photon b into the input modes b_1 and b_2 of the S-CNOT gate. The evolution of the system composed of the photon a, b , and the atomic ensemble E_s in $|\varphi_s\rangle_3 \otimes |\varphi\rangle_b$ is similar to that of $|\varphi_s\rangle_1$. One can get the system in the state $|\varphi_s\rangle_4$ after the photon b leaves the S-CNOT gate,

$$|\varphi_s\rangle_4 = (\beta_1|H\rangle - \beta_2|V\rangle) \otimes (v_1|H\rangle - v_2|V\rangle) \otimes [\alpha_2|a_2\rangle \otimes |g_0^s\rangle \otimes (\mu_1|b_2\rangle + \mu_2|b_1\rangle) + \alpha_1|a_1\rangle \otimes |g_1^s\rangle \otimes (\mu_1|b_1\rangle + \mu_2|b_2\rangle)]. \quad (19)$$

To complete the S-CNOT gate, one has to implement another Hadamard operation H_m followed by a state measurement on the atomic ensemble E_s . If the outcome of the measurement on the atomic ensemble is the state $|g_1^s\rangle$, the composite system will be projected into

$$|\varphi_s\rangle_5 = (\beta_1|H\rangle - \beta_2|V\rangle) \otimes (v_1|H\rangle - v_2|V\rangle) \otimes [\alpha_2|a_2\rangle \otimes \sigma_{x_s^b}|\varphi\rangle_{b_s} + \alpha_1|a_1\rangle \otimes |\varphi\rangle_{b_s}]. \quad (20)$$

With a single phase-flip operation $\sigma_{z_p} = |H\rangle\langle H| - |V\rangle\langle V|$ on photon a and b , the photonic state $|\varphi_s\rangle_5$ changes into the state that is identical to the outcome of the S-CNOT gate with the

spatial DOF of photon a as the control qubit and that of b as the target qubit. As for the $|g_0^s\rangle$ case, the S-CNOT gate can also be accomplished, when an additional single phase-flip operator $\sigma_{z_a} = |a_1\rangle\langle a_1| - |a_2\rangle\langle a_2|$ on the spatial DOF of photon a is performed.

C. The performance of our hyper-CNOT gate

Since the S-CNOT gate and the P-CNOT gate can be implemented individually on the respective DOF of a two-photon system, leaving the other DOF identical to the original one, one can construct the hyper-CNOT gate by applying the P-CNOT gate and the S-CNOT gate successively on the photons a and b . In the ideal case, the hyper-CNOT gate will work deterministically and without error as the P-CNOT gate and the S-CNOT gate do. However, in practice, the birefringence for such combined magnon-cavity system is imperfect as that in most cavity-based optical quantum computation [14,16,17,31], and the deterministic reflection and transmission, respectively, adopted in the strong-coupling regime and the uncoupled situation have to be amended a little, leading to an imperfect hyper-CNOT gate with practical experimental technology [33–36].

In what follows, we quantitatively characterize the efficiency and fidelity of the P-CNOT gate and the S-CNOT gate, respectively. Due to the spontaneous emission of the collective states $|\varphi_i^e\rangle$ ($i = 0, 1$), the photons input into the P-CNOT and S-CNOT gates can be lost, leading to vanish output. The efficiency η which is defined as the probability that both of the input photons will be emitted out from their respect output ports is dependent on the initial states of the input photons. Even if both input photons are emitted by the P-CNOT and the S-CNOT gates, the frequency-dependent reflection and transmission of the input photon will modify the output states of the quantum gates. Besides, the fidelity $F = |\langle \varphi^i | \varphi^p \rangle|^2$ also depends on the initial states of the input photons, where $|\varphi^i\rangle$ and $|\varphi^p\rangle$ stand for the ideal output state and the practical output state, respectively. Since the difference between the two output coupling rates κ_Δ of the asymmetric double-sided cavity could be very little by the use of mirrors with almost identical reflectivity [45–48], we would like to take the symmetric cavity to consider the influence of the detuning and finite magnon-cavity coupling strength on our proposal. To discuss the sensitivity of our proposal to the cavity outcoupling imbalance, we also give out the performance of our hyper-CNOT gate under the asymmetric cavity with $\kappa_\Delta = 0.1\kappa_b$ by choosing $\kappa_c \geq \kappa_b$.

When the control photon a is in a superposition state $|\varphi_a\rangle = 1/2(|a_1\rangle + |a_2\rangle) \otimes (|H\rangle + |V\rangle)$ and the target photon b is in $|\varphi_b\rangle = (\mu_1|b_1\rangle + \mu_2|b_2\rangle) \otimes (v_1|H\rangle + v_2|V\rangle)$, the efficiency of the P-CNOT gate is

$$\eta_p = \frac{1}{2} \{ \xi_0 [|(T_+ + 1)\mu_1|^2 + |\mu_1|^2 + |T_-\mu_2|^2] + \xi_1 [|(T_+ + 1)\mu_2|^2 + |\mu_2|^2 + |T_-\mu_1|^2] \}, \quad (21)$$

with $T_\pm = t_0 \pm t_1$ and $\xi_i = 2[|t_i|^2 + \text{Re}(t_i)]|v_1 + v_2|^2 + 1$ ($i = 0$ or 1). t_1 and t_0 signify the transmission coefficients $t(\omega)$ for $\lambda_i \neq 0$ and $t_0(\omega)$ for $\lambda_i = 0$, respectively. Meanwhile, the fidelity of the optical P-CNOT gate with respect to the initial

state of the photons a and b can be detailed as

$$F_p = \frac{||\mu_1|^2 \zeta_0 - |\mu_2|^2 \zeta_1 + T_- [|\mu_1|^2 \zeta_1 - |\mu_2|^2 \zeta_0]|^2}{4\eta_p}, \quad (22)$$

where $\zeta_0 = 2(t_0 + 1)\text{Re}(v_1 v_2) + t_0$ and $\zeta_1 = 2t_1\text{Re}(v_1 v_2) + t_1 + 1$.

If the input photonic state for the S-CNOT gate is identical to that for the P-CNOT gate, i.e., $|\varphi_a\rangle \otimes |\varphi_b\rangle$, the performance of the S-CNOT gate can be evaluated in a similar way. The efficiency η_s and the fidelity F_s of the S-CNOT gate can be detailed as

$$\eta_s = \frac{1}{2} \{ \xi'_0 [|(T_+ + 1)v_2|^2 + |v_2|^2 + |T_- v_1|^2] + \xi'_1 [|(T_+ + 1)v_1|^2 + |v_1|^2 + |T_- v_2|^2] \}, \quad (23)$$

$$F_s = \frac{||v_1|^2 \zeta'_1 - |v_2|^2 \zeta'_0 + T_- [|v_1|^2 \zeta'_0 - |v_2|^2 \zeta'_1]|^2}{4\eta_s}. \quad (24)$$

Here the parameters $\xi'_i = 2[|t_i|^2 + \text{Re}(t_i)]|\mu_1 + \mu_2|^2 + 1$ ($i = 0$ or 1), $\zeta'_0 = 2(t_0 + 1)\text{Re}(\mu_1 \mu_2) + t_0$, and $\zeta'_1 = 2t_1\text{Re}(\mu_1 \mu_2) + t_1 + 1$.

To evaluate the performance of our schemes, we calculate the average efficiencies $\bar{\eta}_p$ and $\bar{\eta}_s$ and the average fidelities \bar{F}_p and \bar{F}_s over the coefficients in the input photonic states. The P-CNOT gate and the S-CNOT gate enjoy the same performance with our input photons, since the coefficients affecting the efficiencies and fidelities will change their performance into each other by exchanging their spatial state and polarization state, detailed in Eqs. (21)–(24), which will eliminate the effects of coefficients when performing the average over the coefficients of the input photons.

The average efficiencies $\bar{\eta}_p$ and $\bar{\eta}_s$ and the average fidelities \bar{F}_p and \bar{F}_s as functions of the normalized photon detuning Δ/κ and the coupling rate λ/κ are shown in Fig. 4 when setting $\gamma = \kappa$. The average fidelities \bar{F}_p and \bar{F}_s approach a steady value limited by the frequency detuning Δ/κ . Although λ/κ varies by a factor of 2, due to the residual thermal motion of the atom in the current experiment, it has little effect on the performance

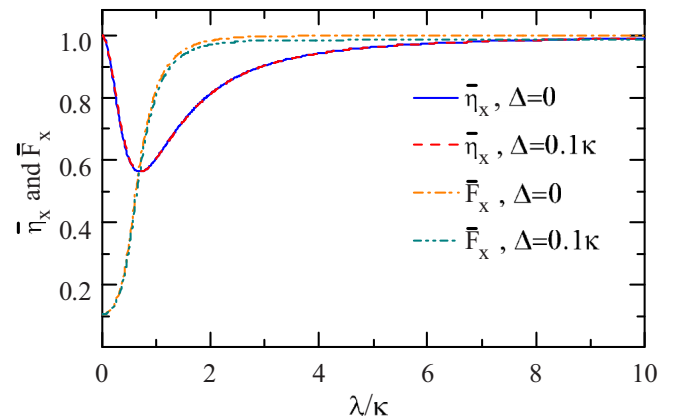


FIG. 4. The efficiencies and fidelities of our P-CNOT and the S-CNOT gates with symmetric double-sided cavities. The solid lines stand for the resonant case and the dotted lines represent the case with $\Delta = 0.1\kappa$ where $\gamma = \kappa$ for practical microcavity.

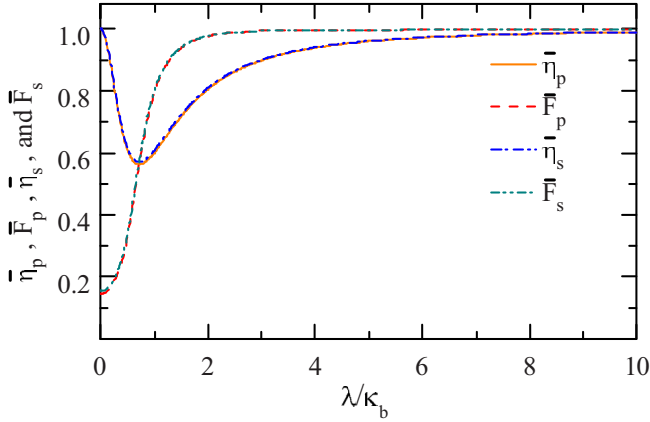


FIG. 5. The average efficiencies and fidelities of our hyper-CNOT gates with asymmetric double-sided cavities. Here the cavity outcoupling rate difference is chosen as $\kappa_\Delta = \kappa_b$, the detuning $\Delta = 0$, and $\gamma = 0.1\kappa_b$.

of our hyper-CNOT gate when λ/κ is large enough. In principle, the detuning Δ/κ can be arbitrarily reduced, if the input photon is tuned to be resonant to the cavity, and then one has $\bar{\eta}_p = \bar{\eta}_s > 90.28\%$ and $\bar{F}_p = \bar{F}_s > 99.64\%$ when $g/\kappa \geq 3$. Even with a detuning as large as $\Delta/\kappa = 0.1$, one can get $\eta_p = \eta_s > 90.26\%$ and $\bar{F}_p = \bar{F}_s > 98.26\%$ when the condition $\lambda/\kappa \geq 3$ is achieved. In other words, the hyper-CNOT gate constituted here, to some extent, is not sensitive to the detuning Δ and the fluctuation of the coupling rate λ/κ .

In the previous discussion, we detailed the performance of our hyper-CNOT gate with a completely symmetric double-sided cavity containing an atomic ensemble. In fact, there might be some difference in the coupling rates between the cavity and modes b_i and c_i ($\kappa_\Delta = \kappa_c - \kappa_b \neq 0$) in practice. To discuss the sensitivity of our scheme to κ_Δ , the average fidelity and average efficiency of our hyper-CNOT gate are calculated with the similar procedure as those used in the symmetric case by using the reflection and transmission coefficients obtained with the asymmetrical cavity, shown in Fig. 5 when setting $\kappa_\Delta = 0.1\kappa_b$ and $\gamma = \kappa_b$ in the resonant case ($\Delta = 0$). The average efficiency $\bar{\eta}_p$ and average fidelity \bar{F}_p of the P-CNOT gate are, respectively, $\bar{\eta}_p > 89.86\%$ and $\bar{F}_p > 99.32\%$ when $\lambda/\kappa_b \geq 3$, and the average efficiency $\bar{\eta}_s$ and average fidelity \bar{F}_s of the S-CNOT gate in this case are, respectively, $\bar{\eta}_s > 90.09\%$ and $\bar{F}_s > 99.33\%$. The little decrease of the average efficiencies and average fidelities in the asymmetric case compared with those in the symmetric case makes our hyper-CNOT gate, to some extent, robust to the cavity outcoupling imbalance.

The parameters above for calculations of efficiencies and fidelities are based on the current experiments achieved with a Bose-Einstein condensate of ^{87}Rb atomic ensemble coupled to an optical Fabry-Perot cavity, where the maximum coupling strength between a single atom and a single intracavity photon, along with the decay rate of the excited state and the cavity mode, are $(\lambda, \kappa, \gamma)/2\pi = (10.6, 1.3, 3)$ MHz [51,52]. Recently, there have been plenty of other methods to couple the atomic ensemble with an optical cavity [53] which might be another building block for our proposal. Therefore, our

hyperparallel quantum computation is robust against the practical imperfections and can be achieved with the current QED setup.

D. Generalized hyper-CNOT^N gate based on the effective Kerr nonlinearity

We only detail the scheme of the two-qubit photonic hyper-CNOT gate in the previous section. However, multiqubit gates are useful, when performing scalable hyperparallel optical quantum computation, since it is resource consuming to constitute the multiqubit gates with building blocks of two-qubit gates and single-qubit gates [2]. Fortunately, our two-qubit hyper-CNOT gate can be easily generalized to multiqubit hyper-CNOT^N gates, where one photon as control qubit and all the others as target qubits, which have been widely researched in the stationary qubit systems [54–57] and could be exploited to perform the hyperentanglement preparation [58], error corrections [59], and quantum algorithms [60,61].

The procedure for constituting the multiqubit photonic hyper-CNOT^N gate could also be divided into two steps: (i) constituting the P-CNOT^N gate on the polarization DOF with the spatial DOF of the photons unaffected; (ii) constituting the S-CNOT^N gate on the spatial DOF with the polarization DOF of the photons unpolluted. We will detail the procedure of the P-CNOT^N gate below, since the S-CNOT^N gate can be achieved individually on the corresponding spatial DOF of the photons, which is similar to that for the P-CNOT^N gate.

Suppose the control photon a is in the superposition state $|\varphi\rangle_a = |\varphi\rangle_{a_s} \otimes |\varphi\rangle_{a_p}$, where the spatial state $|\varphi\rangle_{a_s} = \alpha_1|a_1\rangle + \alpha_2|a_2\rangle$ and the polarization state $|\varphi\rangle_{a_p} = \beta_1|H\rangle + \beta_2|V\rangle$ with $|\alpha_1|^2 + |\alpha_2|^2 = 1$ and $|\beta_1|^2 + |\beta_2|^2 = 1$. The N target photons b^1, b^2, \dots , and b^N are, respectively, in the superposition states of the form $|\varphi\rangle_{b^i} = |\varphi\rangle_{b^i_s} \otimes |\varphi\rangle_{b^i_p}$, where $|\varphi\rangle_{b^i_s} = \mu_1^i|b_1\rangle + \mu_2^i|b_2\rangle$ and $|\varphi\rangle_{b^i_p} = \nu_1^i|H\rangle + \nu_2^i|V\rangle$ with $|\mu_1^i|^2 + |\mu_2^i|^2 = 1$ and $|\nu_1^i|^2 + |\nu_2^i|^2 = 1$. To implement the P-CNOT^N gate, we could use the circuit setup in Fig. 2 by substituting the target photon b in the original P-CNOT gate with the photon string b^1, b^2, \dots , and b^N . Besides, the target photon b^{i+1} should be subsequently input into the cavity after b^i is output by the cavity. Meanwhile, the time delay between each two target photons b^i and b^{i+1} could be utilized to discriminate their spatial modes.

We first initialize the atomic ensemble into the superposition state $|\varphi\rangle_m = \frac{1}{\sqrt{2}}(|g_0^s\rangle + |g_1^s\rangle)$ and then input the control photon a in the state $|\varphi\rangle_a$. After passing through the setup in Fig. 2, with an additional Hadamard operation H_m on the atomic ensemble E_p , the combined photon-ensemble system constituted by photon a and E_p evolves into the state $|\varphi_p\rangle_4$, shown in Eq. (14). Subsequently, we input the first target photon b^1 with its spatial mode, respectively, into the imports b_1 and b_2 as we did for the target photon b during the P-CNOT procedure. After the photon b^1 passes through the setup and propagates into the output modes b_1 and b_2 , the composite system composed of photons a and b^1 and the ensemble E_p evolves into

$$|\varphi_p^N\rangle_1 = [-\beta_2|V\rangle|\varphi\rangle_{b^1_p}|g_0^s\rangle + \beta_1|H\rangle\sigma_{x_p^1}|g_1^s\rangle] \otimes |\varphi\rangle_{a_s} \otimes |\varphi\rangle_{b^1_s}. \quad (25)$$

With a similar procedure, one could subsequently input the target photon b^i after the photon b^{i-1} is emitted by the cavity. The constituted system composed of photons a and $b^1 b^2 \dots b^i$, and the ensemble E_p evolves into

$$|\varphi_p^N\rangle_2 = \left[\beta_1 |H\rangle |g_1^s\rangle \prod_{j=1}^i \sigma_{x_{b_j}^p} + (-1)^i \beta_2 |V\rangle |g_0^s\rangle \right] \otimes |\varphi\rangle_a |\varphi\rangle_{b^1} |\varphi\rangle_{b^2} \dots |\varphi\rangle_{b^i}. \quad (26)$$

Here the operator $\prod_{j=1}^i \sigma_{x_{b_j}^p} = \sigma_{x_{b^1}^p} \otimes \sigma_{x_{b^2}^p} \otimes \dots \otimes \sigma_{x_{b^i}^p}$ represents the bit-flip operation on j th target photons. After all the N target photons pass through the setup, another Hadamard operation H_m on the atomic ensemble E_p is performed, and then the state of the composite system evolves into

$$|\varphi_p^N\rangle_3 = \left\{ \left[\beta_1 |H\rangle \prod_{j=1}^N \sigma_{x_{b_j}^p} + (-1)^i \beta_2 |V\rangle \right] |g_0^s\rangle + \left[-\beta_1 |H\rangle \prod_{j=1}^N \sigma_{x_{b_j}^p} + (-1)^i \beta_2 |V\rangle \right] |g_1^s\rangle \right\} \otimes |\varphi\rangle_a |\varphi\rangle_{b^1} |\varphi\rangle_{b^2} \dots |\varphi\rangle_{b^N}. \quad (27)$$

To decouple the atomic ensemble, a measurement on the ensemble is performed [49,50]. When the outcome is $|g_0^s\rangle$, one can project the $N+1$ photons into the state

$$|\varphi_p^N\rangle_4 = \left[\beta_1 |H\rangle \prod_{j=1}^N \sigma_{x_{b_j}^p} + (-1)^i \beta_2 |V\rangle \right] \otimes |\varphi\rangle_a |\varphi\rangle_{b^1} |\varphi\rangle_{b^2} \dots |\varphi\rangle_{b^N}, \quad (28)$$

which is the desired outcome of the P-CNOT^N gate when the polarization DOF of photon a acts as the control qubit and that of $b^1 b^2 \dots b^N$ as the target qubits, conditioned on N is even. If N is odd, a single phase-flip operator $\sigma_{z_a}^p = |H\rangle\langle H| - |V\rangle\langle V|$ performed on a leads to the same result as that for the even case. When the outcome of the measurement on atomic ensemble is $|g_0^s\rangle$, the P-CNOT^N gate can also be completed with or without a single phase-flip $\sigma_{z_a}^p$ operation on the photon a .

The S-CNOT^N gate on the spatial DOF of the photons could be constituted with the setup in Fig. 3. The procedure of the S-CNOT^N gate can be completed in a similar way to that for P-CNOT^N gate, since the polarization modes of photons involved in the S-CNOT^N gate decouple from the spatial modes and serve a similar function as the spatial modes do in the P-CNOT^N gate. That is, the multiqubit hyper-CNOT^N gate on both DOFs of the photons are achievable, when successively operating the control photon a and the target photons b^1, b^2, \dots , and b^N , with the two CNOT^N gates.

IV. DISCUSSION AND SUMMARY

The interaction between the atomic ensemble and the polarized photon provides us a useful interface for constructing the blocks of hyperparallel photonic quantum computation, since the birefringent propagation of the successively input photons acts as the effective Kerr nonlinearity. The collective

spin wave operations in atomic ensembles are well developed [62], and the fidelities of the spin wave rotation procedures of 99% are reported [63]. Moreover, the atomic ensemble can offer a quantum storage media [35] with multiple modes for the hyperencoded photons [64]. As the control photon and the target photon are injected successively into the magnon-cavity system for the hyper-CNOT gate, a time delay of a few μ s between them is needed, which could be achieved through simple fiber loops. For longer time delay, the atomic ensemble could be utilized to store the coherent state of light for a few minutes [65].

Our two-qubit hyper-CNOT gate is quite efficient, since it enjoys the same advantages as the original ones did [16,17] by hyperencoding a single photon with two qubits by both its spatial and polarization DOFs, which makes the schemes less decoherent than two-photon entanglement, and is relatively easier to perform quantum logical gates on qubits residing in different DOFs of the same photon. In addition, our hyper-CNOT gate is quite different from the previous ones based on the quantum dot embedded in microcavities [16,17] and that assisted by NV centers embedded in photonic crystal cavities coupled to two wave guides [18]. It is more flexible, by dividing the hyper-CNOT gate into the individual S-CNOT gate and the P-CNOT gate. Meanwhile, it could be directly generalized into the multiqubit hyper-CNOT^N gate, which is of great importance when performing the hyperentanglement preparation and redundant encoding procedure [58,66,67], and could find potential application in memoryless quantum communication [68,69] in a hyperparallel quantum network. In addition, it needs only two atomic ensembles in our multiqubit hyper-CNOT^N gate, and it makes our scheme more efficient and more convenient when compared with the multiqubit gate constituted with two-qubit gates and single-qubit gates [2]. Besides, the atomic ensembles are well developed quantum memory systems for photonic qubits, and they can store hyperencoded photons in a single atomic ensemble with longer time of several milliseconds [70], which is essential in quantum networks.

In summary, the effective Kerr nonlinearity induced by an atomic ensemble embedded in a double-sided cavity was proposed based on the input-output theory of the cavity QED. By hyperencoding two qubits in the spatial and polarization DOFs of each photon, a hyperparallel optical quantum computation can be implemented with auxiliary magnon-cavity systems. The proposed scheme is robust to the variation of coupling rate λ_i and the detuning Δ involved in the practical experiment. Maybe this work will be useful for its value in quantum computation and quantum networks with single photons of multiple DOFs.

ACKNOWLEDGMENTS

This work is supported by the National Natural Science Foundation of China under Grants No. 11175094 and No. 91221205, the National Basic Research Program of China under Grant No. 2015CB921002, and the China Postdoctoral Science Foundation under Grant No. 2015M571011. G.L. acknowledges support from the Center of Atomic and Molecular Nanosciences, Tsinghua University.

- [1] M. A. Nielsen and I. L. Chuang, *Quantum Computation and Quantum Information* (Cambridge University Press, Cambridge, UK, 2000).
- [2] A. Barenco, C. H. Bennett, R. Cleve, D. P. DiVincenzo, N. Margolus, P. Shor, T. Sleator, J. A. Smolin, and H. Weinfurter, *Phys. Rev. A* **52**, 3457 (1995).
- [3] N. A. Gershenfeld and I. L. Chuang, *Science* **275**, 350 (1997).
- [4] I. L. Chuang, N. Gershenfeld, M. G. Kubinec, and D. W. Leung, *Proc. R. Soc. London, Ser. A* **454**, 447 (1998).
- [5] G. R. Feng, G. F. Xu, and G. L. Long, *Phys. Rev. Lett.* **110**, 190501 (2013).
- [6] A. O. Niskanen, J. J. Vartiainen, and M. M. Salomaa, *Phys. Rev. Lett.* **90**, 197901 (2003).
- [7] M. Hua, M. J. Tao, F. G. Deng, and G. L. Long, *Sci. Rep.* **5**, 14541 (2015).
- [8] D. Loss and D. P. DiVincenzo, *Phys. Rev. A* **57**, 120 (1998).
- [9] A. Imamoglu, D. D. Awschalom, G. Burkard, D. P. DiVincenzo, D. Loss, M. Sherwin, and A. Small, *Phys. Rev. Lett.* **83**, 4204 (1999).
- [10] H. R. Wei and F. G. Deng, *Sci. Rep.* **4**, 7551 (2014).
- [11] I. L. Chuang and Y. Yamamoto, *Phys. Rev. A* **52**, 3489 (1995).
- [12] P. Kok, W. J. Munro, K. Nemoto, T. C. Ralph, J. P. Dowling, and G. J. Milburn, *Rev. Mod. Phys.* **79**, 135 (2007).
- [13] E. Knill, R. Laflamme, and G. J. Milburn, *Nature (London)* **409**, 46 (2001).
- [14] H. R. Wei and F. G. Deng, *Opt. Express* **21**, 17671 (2013).
- [15] M. A. Ciampini, A. Orioux, S. Paesani, F. Sciarrino, G. Corrielli, A. Crespi, R. Ramponi, R. Osellame, and P. Mataloni, *Light: Sci. Appl.* **5**, e16064 (2016).
- [16] B. C. Ren, H. R. Wei, and F. G. Deng, *Laser Phys. Lett.* **10**, 095202 (2013).
- [17] B. C. Ren and F. G. Deng, *Sci. Rep.* **4**, 4623 (2014).
- [18] B. C. Ren, G. Y. Wang, and F. G. Deng, *Phys. Rev. A* **91**, 032328 (2015).
- [19] F. W. Strauch, *Phys. Rev. A* **84**, 052313 (2011).
- [20] M. Hua, M. J. Tao, and F. G. Deng, *Phys. Rev. A* **90**, 012328 (2014).
- [21] M. Hua, M. J. Tao, and F. G. Deng, *Sci. Rep.* **5**, 9274 (2015).
- [22] F. Jelezko, T. Gaebel, I. Popa, M. Domhan, A. Gruber, and J. Wrachtrup, *Phys. Rev. Lett.* **93**, 130501 (2004).
- [23] H. R. Wei and F. G. Deng, *Phys. Rev. A* **88**, 042323 (2013).
- [24] N. J. Cerf, C. Adami, and P. G. Kwiat, *Phys. Rev. A* **57**, R1477 (1998).
- [25] P. Kok, H. Lee, and J. P. Dowling, *Phys. Rev. A* **66**, 063814 (2002).
- [26] N. Matsuda, R. Shimizu, Y. Mitsumori, H. Kosaka, and K. Edamatsu, *Nat. Photon.* **3**, 95 (2009).
- [27] I. Friedler, D. Petrosyan, M. Fleischhauer, and G. Kurizki, *Phys. Rev. A* **72**, 043803 (2005).
- [28] S. Sevinçli, N. Henkel, C. Ates, and T. Pohl, *Phys. Rev. Lett.* **107**, 153001 (2011).
- [29] T. Peyronel, O. Firstenberg, Q. Y. Liang, S. Hofferberth, A. V. Gorshkov, T. Pohl, M. D. Lukin, and V. Vuletić, *Nature (London)* **488**, 57 (2012).
- [30] Q. A. Turchette, C. J. Hood, W. Lange, H. Mabuchi, and H. J. Kimble, *Phys. Rev. Lett.* **75**, 4710 (1995).
- [31] L. M. Duan and H. J. Kimble, *Phys. Rev. Lett.* **92**, 127902 (2004).
- [32] M. Saffman, T. G. Walker, and K. Mølmer, *Rev. Mod. Phys.* **82**, 2313 (2010).
- [33] Y. Colombe, T. Steinmetz, G. Dubois, F. Linke, D. Hunger, and J. Reichel, *Nature (London)* **450**, 272 (2007).
- [34] K. W. Murch, K. L. Moore, S. Gupta, and D. M. Stamper-Kurn, *Nat. Phys.* **4**, 561 (2008).
- [35] H. Tanji, S. Ghosh, J. Simon, B. Bloom, and V. Vuletić, *Phys. Rev. Lett.* **103**, 043601 (2009).
- [36] M. Wolke, J. Klinner, H. Keßler, and A. Hemmerich, *Science* **337**, 75 (2012).
- [37] D. A. Steck, Rubidium 87 D Line Data, <http://steck.us/alkalidata>, revision 2.1.4, 23 December 2010.
- [38] C. Y. Shih and M. S. Chapman, *Phys. Rev. A* **87**, 063408 (2013).
- [39] D. F. Walls and G. J. Milburn, *Quantum Optics* (Springer-Verlag, Berlin, 1994).
- [40] F. Mei, M. Feng, Y. F. Yu, and Z. M. Zhang, *Phys. Rev. A* **80**, 042319 (2009).
- [41] S. Li, Z. Xu, H. Zheng, X. Zhao, Y. Wu, H. Wang, C. Xie, and K. Peng, *Phys. Rev. A* **84**, 043430 (2011).
- [42] P. Böhi, M. F. Riedel, J. Hoffrogge, J. Reichel, T. W. Hänsch, and P. Treutlein, *Nat. Phys.* **5**, 592 (2009).
- [43] C. K. Law, S. Y. Zhu, and M. S. Zubairy, *Phys. Rev. A* **52**, 4095 (1995).
- [44] L. F. Wei, Y. X. Liu, C. P. Sun, and F. Nori, *Phys. Rev. Lett.* **97**, 237201 (2006).
- [45] A. Muller, E. B. Flagg, J. R. Lawall, and G. S. Solomon, *Opt. Lett.* **35**, 2293 (2010).
- [46] G. Biedermann, F. Benito, K. Fortier, D. Stick, T. Loyd, P. Schwindt, C. Nakakura, R. Jarecki Jr., and M. Blain, *Appl. Phys. Lett.* **97**, 181110 (2010).
- [47] K. M. Birnbaum, A. Boca, R. Miller, A. D. Boozer, T. E. Northup, and H. J. Kimble, *Nature (London)* **436**, 87 (2005).
- [48] A. Kubanek, A. Ourjoumtsev, I. Schuster, M. Koch, P. W. H. Pinkse, K. Murr, and G. Rempe, *Phys. Rev. Lett.* **101**, 203602 (2008).
- [49] J. Volz, R. Gehr, G. Dubois, J. Estève, and J. Reichel, *Nature (London)* **475**, 210 (2011).
- [50] N. Sangouard, C. Simon, H. de Riedmatten, and N. Gisin, *Rev. Mod. Phys.* **83**, 33 (2011).
- [51] F. Brennecke, T. Donner, S. Ritter, T. Bourdel, M. Köhl, and T. Esslinger, *Nature (London)* **450**, 268 (2007).
- [52] F. Brennecke, S. Ritter, T. Donner, and T. Esslinger, *Science* **322**, 235 (2008).
- [53] H. Ritsch, P. Domokos, F. Brennecke, and T. Esslinger, *Rev. Mod. Phys.* **85**, 553 (2013).
- [54] G. W. Lin, X. B. Zou, X. M. Lin, and G. C. Guo, *Phys. Rev. A* **79**, 064303 (2009).
- [55] C. P. Yang, S. B. Zheng, and F. Nori, *Phys. Rev. A* **82**, 062326 (2010).
- [56] H. F. Wang, A. D. Zhu, and S. Zhang, *Opt. Lett.* **39**, 1489 (2014).
- [57] C. P. Yang, Q. P. Su, F. Y. Zhang, and S. B. Zheng, *Opt. Lett.* **39**, 3312 (2014).
- [58] M. Šasšura and V. Bužek, *Phys. Rev. A* **64**, 012305 (2001).
- [59] T. H. Taminiau, J. Cramer, T. van der Sar, V. V. Dobrovitski, and R. Hanson, *Nat. Nanotech.* **9**, 171 (2014).
- [60] T. Beth and M. Rötteler, *Springer Tracts Mod. Phys.* **173**, 96 (2001).
- [61] Y. Lu, G. R. Feng, Y. S. Li, and G. L. Long, *Sci. Bull.* **60**, 241 (2015).
- [62] Z. Xu, Y. Wu, H. Liu, S. Li, and H. Wang, *Phys. Rev. A* **88**, 013423 (2013).

- [63] J. Rui, Y. Jiang, B. Zhao, X. H. Bao, and J. W. Pan, [arXiv: 1501.07067v1](#).
- [64] H. N. Dai, H. Zhang, S. J. Yang, T. M. Zhao, J. Rui, Y. J. Deng, L. Li, N. L. Liu, S. Chen, X. H. Bao, X. M. Jin, B. Zhao, and J. W. Pan, *Phys. Rev. Lett.* **108**, 210501 (2012).
- [65] Y. O. Dudin, L. Li, and A. Kuzmich, *Phys. Rev. A* **87**, 031801(R) (2013).
- [66] Y. B. Sheng and L. Zhou, *Sci. Rep.* **5**, 13453 (2015).
- [67] L. Zhou and Y. B. Sheng, *Phys. Rev. A* **92**, 042314 (2015).
- [68] W. J. Munro, A. M. Stephens, S. J. Devitt, K. A. Harrison, and K. Nemoto, *Nat. Photon.* **6**, 777 (2012).
- [69] S. Muralidharan, J. Kim, N. Lütkenhaus, M. D. Lukin, and L. Jiang, *Phys. Rev. Lett.* **112**, 250501 (2014).
- [70] A. I. Lvovsky, B. C. Sanders, and W. Tittel, *Nat. Photon.* **3**, 706 (2009).